RESEARCH

The PARP1 selective inhibitor saruparib (AZD5305) elicits potent and durable antitumor activity in patient-derived *BRCA1/2*-associated cancer models

Andrea Herencia-Ropero[1,2], Alba Llop-Guevara[1*], Anna D. Staniszewska[3], Joanna Domènech-Vivó[4,5], Eduardo García-Galea[6], Alejandro Moles-Fernández[7,8], Flaminia Pedretti[1], Heura Domènech[1], Olga Rodríguez[1], Marta Guzmán[1], Enrique J. Arenas[9,10,11], Helena Verdaguer[12,13], Fernando J. Calero-Nieto[3], Sara Talbot[3], Luis Tobalina[3], Elisabetta Leo[3], Alan Lau[3], Paolo Nuciforo[14], Rodrigo Dienstmann[6], Teresa Macarulla[12,13], Joaquín Arribas[9,10,15,16,17], Orland Díez[4,8], Sara Gutiérrez-Enríquez[4], Josep V. Forment[3], Mark J. O'Connor[3], Mark Albertella[3], Judith Balmaña[4,18*] and Violeta Serra[1*] [ID]

Abstract

Background Poly (ADP-ribose) polymerase 1 and 2 (PARP1/2) inhibitors (PARPi) are targeted therapies approved for homologous recombination repair (HRR)-deficient breast, ovarian, pancreatic, and prostate cancers. Since inhibition of PARP1 is sufficient to cause synthetic lethality in tumors with homologous recombination deficiency (HRD), PARP1 selective inhibitors such as saruparib (AZD5305) are being developed. It is expected that selective PARP1 inhibition leads to a safer profile that facilitates its combination with other DNA damage repair inhibitors. Here, we aimed to characterize the antitumor activity of AZD5305 in patient-derived preclinical models compared to the first-generation PARP1/2 inhibitor olaparib and to identify mechanisms of resistance.

Methods Thirteen previously characterized patient-derived tumor xenograft (PDX) models from breast, ovarian, and pancreatic cancer patients harboring germline pathogenic alterations in *BRCA1*, *BRCA2*, or *PALB2* were used to evaluate the efficacy of AZD5305 alone or in combination with carboplatin or an ataxia telangiectasia and Rad3 related (ATR) inhibitor (ceralasertib) and compared it to the first-generation PARPi olaparib. We performed DNA and RNA sequencing as well as protein-based assays to identify mechanisms of acquired resistance to either PARPi.

Results AZD5305 showed superior antitumor activity than the first-generation PARPi in terms of preclinical complete response rate (75% vs. 37%). The median preclinical progression-free survival was significantly longer in the AZD5305-treated group compared to the olaparib-treated group (> 386 days vs. 90 days). Mechanistically, AZD5305 induced more replication stress and genomic instability than the PARP1/2 inhibitor olaparib in PARPi-sensitive tumors. All

*Correspondence:
Alba Llop-Guevara
alballop@gmail.com
Judith Balmaña
jbalmana@vhio.net
Violeta Serra
vserra@vhio.net
Full list of author information is available at the end of the article

tumors at progression with either PARPi (39/39) showed increase of HRR functionality by RAD51 foci formation. The most prevalent resistance mechanisms identified were the acquisition of reversion mutations in *BRCA1/BRCA2* and the accumulation of hypomorphic BRCA1. AZD5305 did not sensitize PDXs with acquired resistance to olaparib but elicited profound and durable responses when combined with carboplatin or ceralasertib in 3/6 and 5/5 models, respectively.

Conclusions Collectively, these results show that the novel PARP1 selective inhibitor AZD5305 yields a potent antitumor response in PDX models with HRD and delays PARPi resistance alone or in combination with carboplatin or ceralasertib, which supports its use in the clinic as a new therapeutic option.

Keywords PARP inhibitors, PARP1 selective, Targeted therapy, Breast cancer, DNA damaging agent, BRCA1/2, RAD51, Homologous recombination deficiency, HRD, Antitumor activity

Background

First-generation poly(ADP-ribose) polymerase inhibitors (PARPi), namely olaparib, talazoparib, niraparib, and rucaparib, have been approved for the treatment of certain ovarian, breast, prostate, and pancreatic cancers [1–14]. PARPi are mostly recommended in a context of homologous recombination repair (HRR) deficiency (HRD) [15, 16], identified either as platinum sensitivity or by the presence of germline/tumor DNA alterations [17]. Currently approved PARPi inhibit both PARP1 and PARP2 (PARP1/2). PARP1/2 enzymes are important DNA damage sensors that bind to the site of damage to recruit repair factors through the formation of branched poly(ADP-ribose) (PAR) chains (PARylation) [18]. PARPi, by inhibiting PARP autoPARylation, prevent its effective release from unrepaired DNA, leading to PARP trapping. As consequence, PARP/DNA complexes stall the progression of DNA replication forks, leading to DNA double strand breaks (DSBs) that, in a context of HRD, cannot be effectively repaired. Thus, these tumors accumulate DNA damage that leads to genomic instability and cell death. Despite their initial benefit, reducing primary and acquired resistance to first-generation PARPi remains a clinical need [19]. In this sense, overcoming PARPi resistance with drugs that target the DNA damage response (DDR) has been previously proposed and it has been shown that the ATR inhibitor (ATRi) ceralasertib resensitizes PARPi-resistant high grade serous ovarian cancer to olaparib [20–22]. In addition, while demonstrating an improved safety profile compared with standard-of-care chemotherapy, treatment with PARPi still results in hematological toxicity such as anemia and neutropenia in 40% and 23% of patients, respectively [23]. Importantly, PARP1 and not PARP2 trapping is sufficient to induce synthetic lethality in cancer cells with HRD [24, 25]. Furthermore, PARP2 has been described to play an essential role in hematopoietic renewal and thus, its inhibition may contribute towards the hematological adverse effects observed in patients treated with first-generation PARPi

[26, 27]. In line with this, saruparib (AZD5305), a highly selective PARP1 inhibitor with potent trapping capacity, has been developed [28, 29]. Selective targeting of PARP1 with AZD5305 displays greater differential antiproliferative effects in HRR-mutant vs. wild type cells, compared to first-generation PARPi. In vivo, AZD5305 also exhibits a more profound antitumor response compared to first-generation PARPi, while reducing levels of hematological adverse effects both alone and in combination with carboplatin in mouse models [29]. In the clinic, the PETRA trial (NCT04644068) is a phase I/IIa clinical trial assessing AZD5305 in monotherapy or in combination with different chemotherapies or with antibody–drug-conjugates. Here, we evaluated the antitumor activity of AZD5305 vs. olaparib and compared AZD5305 as single agent and its combination with carboplatin or with an ATRi in PDX models with *BRCA1*, *BRCA2* (*BRCA1/2*), or *PALB2* mutations. We also investigated potential differences in the mode of action and mechanisms of resistance following PARP1 vs. PARP1/2 inhibition.

Methods

Patient samples and clinical annotations

In this exploratory analysis, 10 PDX were used, derived from patients with HRR-related breast (triple negative, ER+, or HER2-positive breast cancer), ovarian (high-grade serous), or pancreatic cancer from patients carrying germline pathogenic variants in *BRCA1*, *BRCA2*, or *PALB2* genes. One ER+BC model was generated from a clinical progression to talazoparib (PDX474.7). PDX196 was generated from the pericardial effusion of an ovarian cancer patient on treatment with PARPi shortly before clinical progression, and PDX168 came from a platinum-refractory pancreatic cancer patient (Additional file 1: Supplementary Table S1). Clinicopathologic characteristics, including sex, race, histological subtype, treatment outcome, and history before and after biopsy for PDX generation, were collected.

Herencia-Ropero *et al. Genome Medicine* (2024) 16:107

Page 3 of 17

Generation of PDX models and in vivo treatment experiments

Fresh tumor samples from patients were collected for implantation into nude mice following the European Union's animal care directive (2010/63/EU) and were approved by the Ethical Committee of Animal Experimentation of the Vall d'Hebron Research Institute. To generate patient-derived xenografts (PDXs), surgical or biopsy specimens from primary tumors or metastatic lesions were immediately implanted in mice. Fragments of 30 to 60 mm^3 were implanted into the lower flank of 6-week-old female athymic Rj:NMRI-*Foxn1*$^{nu/nu}$ (Janvier) mice. Animals were housed in air-filtered laminar flow cabinets with a 12-h light cycle and food and water ad libitum. Mice bearing breast cancer models were supplemented with 1.5 μM 17β-estradiol (Sigma-Aldrich) in drinking water. Upon growth of the engrafted tumors, models were perpetuated by serial transplantation. In each passage, flash-frozen and formalin-fixed, paraffin-embedded (FFPE) samples were taken for genotyping and histological analyses.

To evaluate the sensitivity to the drugs, tumor-bearing mice were equally distributed into treatment groups with tumors ranging 100 to 300 mm^3. AZD5305 (saruparib) and olaparib were administered orally (p.o.) six times per week in water/HCl pH 3.5–4 at 1 mg/kg and 10% v/v DMSO/10% w/v Kleptose [HP-β-CD] at 100 mg/kg, respectively. AZD6738 was administered p.o. five times per week in 10% v/v DMSO, 40% v/v PEG300 at 25 mg/kg. Carboplatin was given intraperitoneally (i.p.) once a week in 0.85% physiologic saline at 37.5 mg/kg. Tumor growth was measured with caliper bi-weekly from first day of treatment. To generate PDX models with acquired resistance to olaparib, treatment was maintained for up to 150 days in olaparib-sensitive tumors until individual tumors regrew or maintained in observation for up to 450 days. In addition, pharmacodynamic experiments were conducted and collected after 12 days of dosing and 2 h after final doses. Tumor volume was calculated as $V = 4\pi/3 \times L \times l^2$, "*L*" being the largest diameter and "*l*" the smallest. In all experiments, mouse weight was recorded twice weekly. Mice were euthanized using carbon dioxide overdose (100% at 5 PSI) for a minimum of 3 min in an euthanasia chamber as recommended by the Euthanasia Guidelines for Investigators. Mice were left undisturbed for an additional 5 min and death was confirmed by cervical dislocation. Euthanasia was performed according to humane endpoints, e.g., when tumors reached 1500 mm^3, in accordance with institutional guidelines.

Evaluation of response to therapy in PDXs

The antitumor activity in therapy-resistant models was determined by comparing individual tumor volumes at 21 days to their respective baseline values: % tumor volume change $= (V_{21days} - V_{initial})/V_{initial} \times 100$. For therapy sensitive PDXs, the best response was defined as the minimum value of % tumor volume change sustained for at least 10 days. To classify the overall response of each PDX, we modified the RECIST (mRECIST) criteria, to be based on the mean % tumor volume change: complete response (CR), best response $< -95\%$; partial response (PR), $-95\% <$ best response $< -30\%$; stable disease (SD), $-30\% <$ best response $< +20\%$, progressive disease (PD), best response $> +20\%$.

Response to therapy was evaluated by measuring different preclinical readouts: preclinical complete response rate (pCRR), preclinical overall response rate (pORR), and preclinical benefit rate (pCBR), calculated over the mean of individual tumors from olaparib-sensitive PDX models showing at least one CR, CR+PR, and CR+PR+SD upon PARPi treatment, respectively. More specifically, pCRR was defined as the fraction of PDXs with at least one individual tumor reaching a CR for at least 10 days. pORR was defined as the fraction of PDXs with at least one individual tumor reaching a CR or a PR for at least 10 days, and pCBR as the fraction of PDXs with at least one individual tumor reaching a CR or a PR for at least 10 days or a SD for a minimum of 80 days. Preclinical progression-free survival (pPFS) was defined as the time to disease progression or death from any cause. Preclinical time to progression (pTTP) was defined as the number of days until initially sensitive tumors (CR+PR+SD) regrew.

Targeted sequencing

All laboratory methods were performed using the manufacturer's protocols. Genomic DNA was isolated from fresh-frozen PDX tissue using the DNeasy Blood & Tissue Kit (Qiagen). All samples were quantified using the Qubit® dsDNA HS Assay Kit (catalog #Q32851) and Qubit 2.0 fluorometer (Thermo Fisher Scientific, Waltham, MA, USA). Hybridization, capture, and sequencing of exonic and intronic regions ($< \pm 10$ bp) of interest were performed using the DNA NGS-based gene panel Hereditary Plus OncoKitDx (Healthincode) in a MiSeq device (Illumina). Bioinformatic analysis of SNVs, insertion/deletions, CNVs, and Alus was performed using Data Genomics software (Imegen; v19.1). Reversion mutations were verified by manual inspection of alignments in IGV. Variants were described and classified according to HGVS (http://www.hgvs.org) and ACMG/GAMP (2015), with reference hg19 (GRCh37).

Herencia-Ropero *et al. Genome Medicine*   (2024) 16:107

Page 4 of 17

No variants were detected in regulatory or intronic zones > ± 10 bp.

Exome sequencing

All laboratory methods were performed using the manufacturer's protocols. Genomic DNA was isolated from fresh-frozen PDX tissue using the DNeasy Blood & Tissue Kit (Qiagen). All samples were quantified using the Qubit® dsDNA BR Assay Kit (Invitrogen; #Q32853) and by Qubit Flex Fluorometer (Invitrogen), DNA purity was determined using a NanoDrop Eight (Thermo Scientific), and DNA integrity was measured using a 4200 Tapestation (Agilent). Exome libraries were constructed using the Illumina DNA Prep with Exome 2.0 Plus Enrichment (Illumina, #20077596). Paired-end sequencing with a read length of 150 bp was performed using Illumina NovaSeq 6000 with approximately 10 Gbp per sample for ~200-fold average sequence depth. Library sizes and quantification were determined by 4200 Tapestation (Agilent) and pooled libraries were subsequently pooled equimolar. Each library was loaded onto one lane of an S4 v1.5 flow cell (300 cycles) (Illumina, #20028312). Sequencing data was demultiplexed, passed through a bcl-to-fastq conversion program (bcl2fastq v2.20.0.422). Fastq files were analyzed using pipeline software bcbio-nextgen v1.2.9 (https://doi.org/https://doi.org/10.5281/zenodo.3564938). Reads were aligned to the human hg38 and mouse mm10 reference using bwa mem v0.7.17, and sequencing duplicates for each UMI were collapsed into a single consensus read using fgbio v1.4.0. All software were run using best practice parameters established within the bcbio workflow or in-house. Mouse-derived sequences were removed using Disambiguate [30]. Variant calling was performed using VarDict v1.8.2 [31], down to a variant allele frequency (VAF) of 1% (before filtering and curation) and variant effects annotated by snpEff 5.0 [32]. Filtering of non-cancer variants (i.e., common polymorphisms) was performed as per VarDict best practice.

Additionally, the following filters were applied using the NGS Report App in SolveBio (https://www.solvebio.com/): preset filter: Tissue; Hide Variant Depth (VD) below: 3; Hide Total Depth below: 50; Additional Solve-Bio filters: "type" does not equal "synonymous_variant" and "dkfzbias" does not equal "strand." Copy number analysis was performed using Seq2C v1.3 [31]. The change in the normalized Log2 values was used to determine potential copy number changes. Chromosome Y was excluded and only deletions with log2ratio < 0 or whole gene amplifications with log2ratio > 0 were kept.

Structural variants were reported by manta v1.6.0 and filtered for having annotation_parsed.detail__exact = ON_PRIORITY_LIST, split_read_support_1 > 15, split_read_support_2 > 15.

RNA sequencing

RNA was extracted from 15 to 30 mg of fresh-frozen tumor from PDX samples by using the RNeasy Mini kit (Qiagen). RNA concentration was determined by Qubit Flex Fluorometer (Invitrogen), RNA purity was determined using a NanoDrop Eight (Thermo Scientific), and RNA integrity was measured using a 4200 Tapestation (Agilent). Libraries were prepared using NEBNext Ultra II Directional RNA Library Prep Kit for Illumina (New England BioLabs, E7760L) or NEBNext® Ultra™ II RNA Library Prep Kit (New England BioLabs, E7770L) as per manufacturer's guidelines. Ribosomal RNA (rRNA) was removed using the NEBNext® Poly(A) mRNA Magnetic Isolation Module (New England BioLabs, E7490L) or using the NEBNext® rRNA Depletion Kit v2 (Human/Mouse/Rat) (New England BioLabs, E7400X). Paired-end sequencing with a read length of 150 bp was performed using Illumina NovaSeq 6000. Library sizes and quantification were determined by 4200 Tapestation (Agilent) and libraries were subsequently pooled equimolar. Each library was loaded onto one lane of an S4 v1.5 flow cell (300 cycles) (Illumina, #20028312).

The RNAseq pipeline implemented in bcbio-nextgen (version 1.2.9) was used for quality control and gene expression quantification. Reads were aligned to the UCSC build GRCh38 *Homo sapiens* genome, augmented with transcript information from Ensembl release 86 using STAR's 2-pass mapping mode (version 2.6.1d), and to mouse mm10 genome. Alignments were evaluated for evenness of coverage, rRNA content, genomic context of alignments, and complexity using a combination of FastQC, Qualimap, and custom tools. Transcripts per million (TPM) measurements per isoform were generated by alignment-based quantification using Salmon (version 1.6.0) and used to estimate abundance of genes [33]. The aggregated gene counts were used for differential gene expression analyses with DESeq2 [34]. Log2 transformation was used for data analysis.

BRCA1 isoforms analysis

RNA was extracted using the RNeasy Mini Kit (Qiagen) with an additional step of DNase digestion using the RNase-Free DNase Set (Qiagen). A total of 200 ng of RNA were retrotranscribed to yield cDNA using the PrimeScript RT reagent kit (Takara), combining random and oligo-dT primers. Quantification of the *BRCA1* Δ11q isoform transcript levels was performed by reverse transcription-quantitative PCR (RT-qPCR) using TaqMan probes targeting exon 11 cryptic donor and exon 12 acceptor junction (custom

Herencia-Ropero *et al. Genome Medicine*   (2024) 16:107

Page 5 of 17

assay). Additionally, a TaqMan probe expanding exon 23–24 (Hs01556193_m1) junction was used to measure *BRCA1* global expression. The geometric means of the expression values for both *RPLP0* (Hs99999902_m1) and *GAPDH* (Hs02758991_g1) housekeeping genes were used to normalize the expression. For each sample, qPCR assays were performed in triplicate using 1 μl of the 20 × TaqMan gene expression assay (TaqMan probes), 10 μl of 2 × TaqMan Fast Advanced Master Mix (Applied Biosystems), 8 μl of water, and 1 μl of the cDNA (20 ng) previously generated. Samples were run for 40 cycles on a QuantStudio 6 Flex PCR System (Applied Biosystems) with the following thermal cycler conditions: 2 min at 50 °C, 20 s at 95 °C, 3 s at 95 °C, and 30 s at 60 °C. Triplicates were individually analyzed, and the corresponding mean values were considered. Data obtained in the form of quantification cycle (Ct) was normalized using the average values of the two reference genes (ΔCt) [35]. Splicing fraction of the Δ11q isoform was calculated as $2^{-\Delta Ct(\Delta 11q)}/(2^{-\Delta Ct(23-24)}) \times 100$ [36]. Samples presenting *BRCA1* Δ11q splicing fraction > 1.5 × the splicing fraction at baseline were classified as hypomorphic BRCA1 due to Δ11q isoform overexpression.

PARylation assay

A frozen tumor specimen was homogenized in ice-cold 1 × radioimmunoprecipitation assay (RIPA) buffer (Tris–HCl pH 8.0 10 mM, EDTA 1 mM, Triton-X-100 0.1%, SDS 0.1%, SDC 0.1%, and NaCl 140 mM) supplemented with 1X protease inhibitor cocktail (cOmplete, Roche), NaF 10 mM, Na2VO4 200 mM, and PMSF 5 mM. Protein concentration was calculated using DC™ Protein Assay (Bio-Rad). PARylation was then determined by western blot. Briefly, a total of 20 μg of protein was used on 8% and 12% SDS-PAGE acrylamide gels at 100 V and transferred to nitrocellulose membrane for 1.5 h at 100 V. Membranes were blocked for 1 h in 5% milk in Tris-buffered saline (TBS) with 0.1% Tween20 (T-TBS) and then hybridized using the corresponding primary antibodies in 5% bovine serum albumin (BSA, Sigma-Aldrich, #A9647) with T-TBS overnight. The rabbit anti-poly/mono(ADP-ribose) (E6F6A) (Cell Signaling #83,732, 1:1000) and human GAPDH (Abcam, ab128915) antibodies were used. Membranes were incubated for 1 h with mouse and rabbit horseradish peroxidase (HRP)-conjugated secondary antibodies (GE Healthcare) in 5% milk in T-TBS. Proteins were detected with Immobilon Western Chemiluminescent HRP substrate (Millipore). Immunoblots were captured at the chemiluminescence imager Amersham Imager 600 (GE Healthcare). Images were captured with FUJIFILM LASS-4000 camera system.

Immunofluorescence and biomarker scoring

The following primary antibodies were used for immunofluorescence (IF): rabbit anti-RAD51 (Abcam ab133534, 1:1000), mouse anti-geminin (NovoCastra NCL-L, 1:60), rabbit anti-geminin (ProteinTech 10,802–1-AP, 1:400), mouse anti-BRCA1 (Santa Cruz Biotechnology sc-6954, 1:50), mouse anti-γ-H2AX (Millipore #05–636, 1:200), rabbit anti-phospho RPA32/RPA2 (S4/S8) (pRPA, Bethyl Laboratories A300-245A, 1:500), and rabbit anti-53BP1 (Cell Signaling 4937, 1:100). Goat anti-rabbit Alexa fluor 568, goat anti-mouse Alexa fluor 488, donkey anti-mouse Alexa fluor 568, and goat anti-rabbit Alexa fluor 488 (all from Invitrogen; 1:500) were used as secondary antibodies. The IF staining was performed on FFPE PDX tumors as described in Castroviejo-Bermejo et al [37].

RAD51, BRCA1, γ-H2AX, and pRPA scores were quantified as the percentage of geminin-positive cells with 5 or more nuclear foci. Geminin is a master regulator of cell-cycle progression that ensures the timely onset of DNA replication and was used as counterstaining to mark for S/G2-cell cycle phase [38]. Samples with low γ-H2AX score (< 25% of positive cells) or with < 40 geminin-positive cells were not evaluated due to insufficient endogenous DNA damage or insufficient tumor cells in the S/G2-phase of the cell cycle, respectively. Progressing tumors with high BRCA1 score (> 1.5 × the percentage of BRCA1 score of the same PDX at baseline) were classified as harboring hypomorphic BRCA1. Recruitment of 53BP1 to DNA damage was evaluated by the qualitative assessment of geminin-positive cells with 5 or more 53BP1 nuclear foci. One hundred geminin-positive cells from at least three representative areas of each sample were analyzed for each biomarker. Genomic instability was scored as the percentage of tumor cells with at least one micronucleus based on DAPI staining (micronuclei score). One hundred cells from at least three representative areas of each sample were analyzed for the micronuclei score. All scorings were performed blindly onto life images using a 60 × -immersion oil lens. At least two biological replicates per PDX model were analyzed.

Statistical analysis

Data was analyzed with GraphPad Prism version 8.2.1 (GraphPad Software) and R software. Shapiro–Wilk test was used to assess normality of data distributions. If the null hypothesis of normal distribution was not rejected, statistical tests were performed using unpaired two-tailed *t*-test (for two groups comparison of RAD51 score). Otherwise, the non-parametric pairwise Wilcoxon test corrected for multiple testing (false discovery

rate correction) was used (for two groups comparison of treatments as percentage of change from baseline) [39]. Bars represent the mean of at least three technical replicates. For preclinical readouts of response (pCRR, pORR, and pCBR), two binomial generalized linear mixed-effects models were performed, both with PDX models as random factor [40]. First, preclinical readouts of response to AZD5305 were analyzed using the response that the same PDX showed upon treatment with olaparib as covariate. The aim of these models was to test whether AZD5305 response rates correlated with olaparib response. Second, a deeper analysis was performed only with those models that showed at least one individual tumor sensitive to olaparib. These models included the preclinical readouts of response as dependent variable and the treatment (olaparib and AZD5305) as fixed factor. In the case of preclinical readouts assessing progression (pPFS and pTTP), a mixed-effects cox regression model was performed [41], all of them in R software [42]. Progression rate of tumors treated with AZD5305 and olaparib was compared using a chi-square test. To calculate the association between RAD51 score and pTTP to both PARPi in PDXs and between RAD51 and BRCA1 scores of progressing tumors, a linear regression model was fitted to estimate the R^2 with 95% confidence intervals (CI). To analyze biomarker (RAD51, BRCA1, γ-H2AX, pRPA, and micronuclei) scores according to response to AZD5305, a linear mixed-effects model was used.

Results

AZD5305 shows potent and durable antitumor response in HRR-altered PDX models

The antitumor activity of saruparib (AZD5305) was evaluated in a panel of 13 PDX models harboring alterations in the homologous recombination repair (HRR) pathway genes: six with pathogenic mutations in *BRCA1*, two in *BRCA2*, and one in *PALB2* (Fig. 1A, Additional file 2: Supplementary Table S2, and Additional file 3: Supplementary Table S3). A dose of 1 mg/kg AZD5305 was chosen as maximum efficacious dose based on previous favorable exposure, antitumor efficacy, and tolerability data [29]. Treatment with AZD5305 revealed antitumor activity in 7 PDX models: complete response (CR) in four PDXs (PDX230, PDX124, PDX474.2, and PDX173), partial response (PR) in two (PDX179 and PDX196), and stable disease (SD) in one PDX (PDX341; Fig. 1A). Of note, PDX179 exhibited a markedly superior response to AZD5305 vs. olaparib. Progression upon treatment with AZD5305 was observed in two models with primary resistance to olaparib (PDX127 and PDX168), likely due to loss of *FAM35A/SHLD2* leading to defects in the 53BP1-Shieldin pathway [43] and lack of gene-specific

loss of heterozygosity (gsLOH) of the *PALB2* pathogenic mutation, respectively (Additional file 2: Supplementary Table S2). The three olaparib-resistant models that had been generated from olaparib-sensitive PDXs after prolonged exposure and steep progression to olaparib (PDX173OR3, PDX230OR5, and PDX474.2OR2) showed resistance to AZD5305, as did the model obtained from the clinical progression to talazoparib (PDX474.7). We identified a plausible mechanism of resistance to olaparib in two models, namely a reversion mutation in *BRCA2* in PDX474.2OR2 and the expression of a potentially hypomorphic BRCA2 protein in PDX474.7 (Additional file 4: Fig. S1 and Additional file 2: Supplementary Table S2) [44]. We did not establish the specific genetic mechanism of resistance to PARPi for PDX173OR3 nor for PDX230OR5, but all resistant models showed RAD51 nuclear foci, suggesting a restoration of the HRR pathway functionality (RAD51 score > 10%, Fig. 1A).

Focusing on PARPi-sensitive tumors, AZD5305 as single agent showed superior antitumor activity than the first-generation PARPi in terms of preclinical CR rate (pCRR, 75%, 95% CI: 50–90% vs. 37%, 95% CI: 18–62%; $p = 0.001$). However, similar preclinical overall response rate (pORR, 94%; 95% CI: 64–99% vs. 88%; 95% CI: 46–98%; $p = 0.11$) and preclinical benefit rate (pCBR, 96%; 95% CI: 75–99% vs. 92%; 95% CI: 64–99%; $p = 0.25$) were observed in AZD5305- and olaparib-treated PDXs (Fig. 1B).

We then sought to investigate the long-term benefit to either PARPi. Consistent with the higher pCRR, a higher percentage of tumors remained in response while on treatment or after treatment discontinuation with AZD5305, compared to olaparib-treated tumors (36/45 (80%) with AZD5305 vs. 20/50 (40%) with olaparib, $p < 0.0001$, Additional file 5: Fig. S2A, S2B and Additional file 6: Supplementary Table S4). In addition, the median preclinical progression-free survival (pPFS) was significantly longer in the AZD5305 group compared to the olaparib group (> 386 days vs. 90 days; hazard ratio for progression or death, 0.39; 95% CI: 0.23–0.66; $p < 0.001$; Fig. 2A and B). The preclinical time to progression (pTTP) was also longer with AZD5305 compared to olaparib in sensitive tumors (172 days vs. 113 days; hazard ratio of 0.51; 95% CI: 0.33–0.78; $p = 0.002$; Fig. 2B and Additional file 5: Fig. S2C). Taken together, these data show that treatment with AZD5305 results in a higher degree of preclinical CR rate and a more durable response than treatment with a first-generation PARPi.

RAD51 foci captures PARPi sensitivity and restoration of HRR functionality

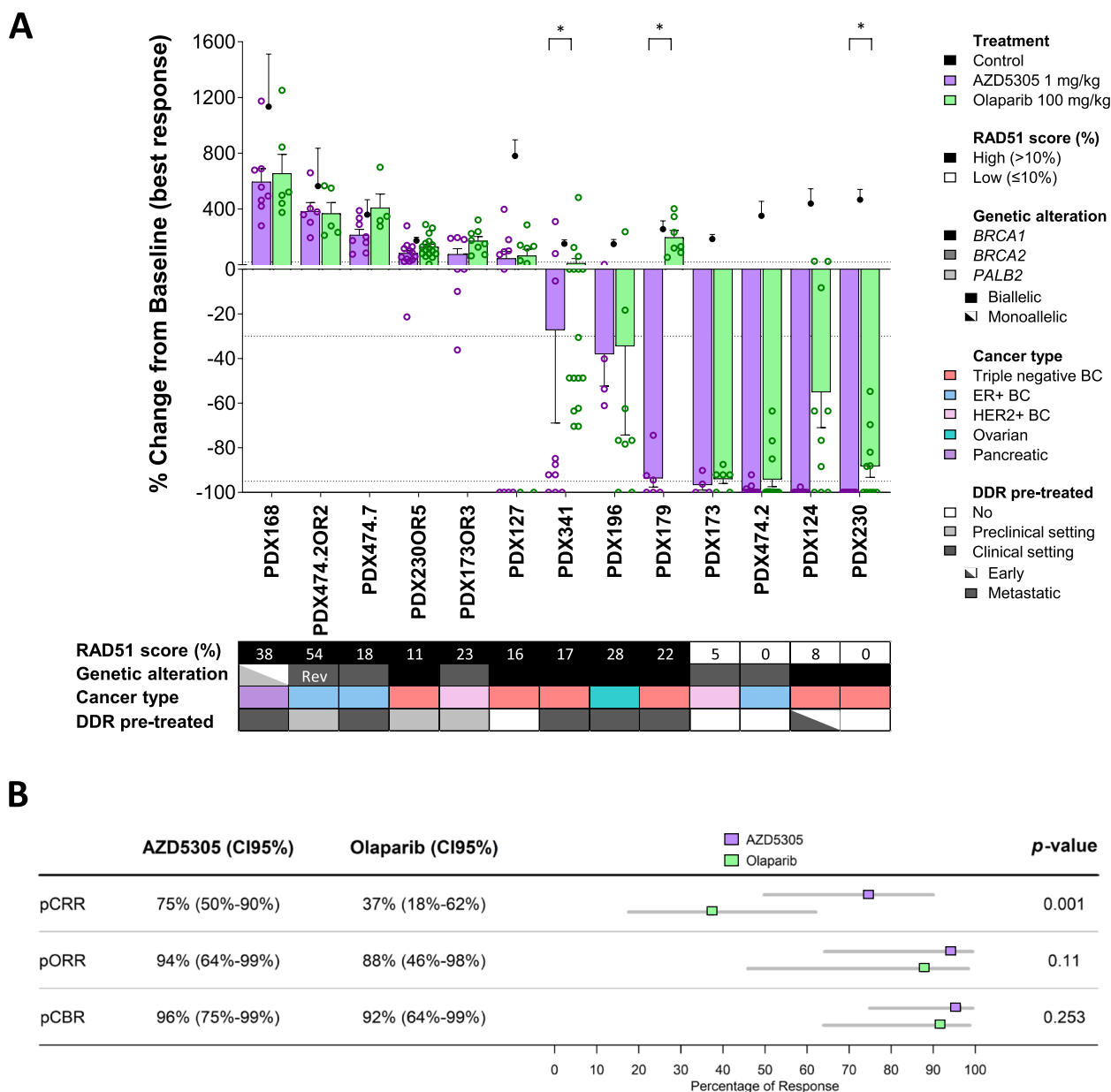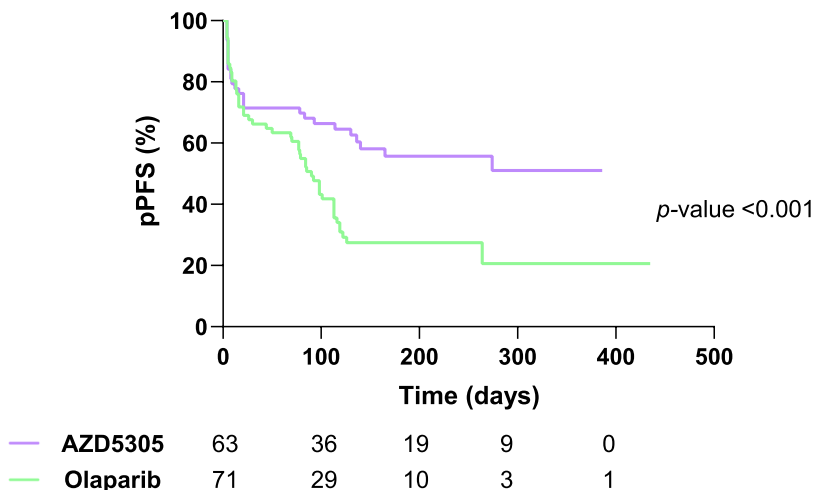We aimed to explore if the functional status of HRD by RAD51 foci was associated with response to PARP1

A

B

Fig. 1 Antitumor activity of AZD5305 and olaparib in PDXs. **A** Waterfall plot showing the antitumor activity of AZD5305 and olaparib in $N=13$ PDX models, measured as percentage of tumor volume change compared with the tumor volume on day 1. Each bar indicates the mean and SEM of at least three biological replicates (open circles). The mean of control tumors ($n \geq 3$) is represented with solid circles. $+20\%$, -30%, and -95% are marked by dotted lines to indicate the range of PD, SD, PR, and CR, respectively. The lower box summarizes the RAD51 score (%), the specific gene alteration harbored by each model and its allelic status, the cancer type, and previous treatment history with DDR drugs in the "Early"-stage vs. "Metastatic" disease setting. Rev, reversion mutation; DDR, DNA damage repair. *p* values, pairwise Wilcoxon test corrected for multiple testing. **B** Comparison of preclinical mRECIST criteria-based readouts to evaluate response to PARPi. pCRR, preclinical complete response rate; pORR, preclinical overall response rate; pCBR, preclinical benefit rate. Percentage of tumors, 95% confidence intervals (CI95%), forest plot, and *p* values (generalized linear mixed-effects model) are shown

selective inhibition [37, 45, 46]. Tumors that were resistant to AZD5305 showed a significantly higher RAD51 score than sensitive tumors (median of 27% vs. 11%, $p=0.046$; Additional file 7: Fig. S3A). Of note, some of the

AZD5305-sensitive models with high levels of RAD51 (>10%) harbor pathogenic alterations in the exon 11 of *BRCA1*, for which PARP1/2 inhibitors can elicit an intermediate antiproliferative response [47]. We also observed

Herencia-Ropero *et al. Genome Medicine*   (2024) 16:107

Page 8 of 17

A

AZD5305	63	36	19	9	0
Olaparib	71	29	10	3	1

B

	Population	AZD5305	Olaparib	HR (CI95%)		*p*-value
pPFS	Sensitive and Resistant	Not Achieved (>386 days)	90 days	0.39 (0.23-0.66)		<0.001
pTTP	Sensitive	172 days	113 days	0.51 (0.33-0.78)		0.002

Fig. 2 Analysis of response to AZD5305 and olaparib in PDXs. **A** Kaplan–Meier curve showing pPFS for AZD5305- and olaparib-treated individual tumors and **B** analysis of response and forest plot for pPFS (%) in PARPi-sensitive and resistant tumors (AZD5305, *n*=63; olaparib, *n*=71) and pTTP in PARPi-sensitive tumors (AZD5305, *n*=45; olaparib, *n*=50). *p* values, mixed-effects Cox model

that the RAD51 score correlated with the pTTP upon AZD5305 and olaparib treatment ($R^2=0.55$, $p=0.004$, and $R^2=0.43$, $p=0.01$), with no differences between both ($p=0.66$, Additional file 7: Fig. S3B and S3C).

We next aimed to gain further insight into the mechanisms leading to acquired resistance. We observed that most acquired-resistant tumors showed enhanced HRR functionality as assessed by RAD51 foci, regardless of the specific PARPi (9/9 AZD5305- (*p* value=0.02) and 28/30 olaparib-progressing tumors (*p* value=0.02); Fig. 3A). Reversion mutations in *BRCA1* or *BRCA2* were seen in 5/30 (17%) tumors that had progressed to olaparib, while no reversions were observed in those progressing to AZD5305 (Fig. 3B, C, and D; Additional file 6: Supplementary Table S4). The prevalence of reversion mutations was high in tumors from certain PDX models, such as the ER+*BRCA2*-mutant model PDX474.2 (Additional file 8: Fig. S4; Additional file 6: Supplementary Table S4). Of note, patient 474 had not received any platinum drug that could have induced subclonal reversion mutations prior to establishing the PDX model. We then aimed to

investigate whether this predisposition was due to an increased mutational rate or increased usage of microhomology mediated end joining (MMEJ) as a backup mechanism to repair DSBs in the absence of HRR [48, 49]. Overall, we did not observe an increased mutational rate in PDX474.2 tumors progressing to PARPi compared to other PARPi-progressing models (Additional file 8: Fig. S4B), but 4/5 (80%) olaparib-progressing tumors with reversion mutations had evidence of microhomology use at the deletion site (Additional file 8: Fig. S4C).

We also investigated the emergence of hypomorphic BRCA1 associated with PARPi resistance, as it has been described that tumors with *BRCA1*-exon 11 mutations are prone to generate splicing isoforms, such as the Δ11q, leading to the expression of a hypomorphic BRCA1 protein and to PARPi resistance [47]. We noted that BRCA1 C-terminal nuclear foci were increased above the baseline levels in two *BRCA1*-exon 11 mutated models (PDX124 and PDX341), namely in 4/5 tumors progressing to AZD5305 and in 14/19 tumors progressing to olaparib, including the individual tumor harboring
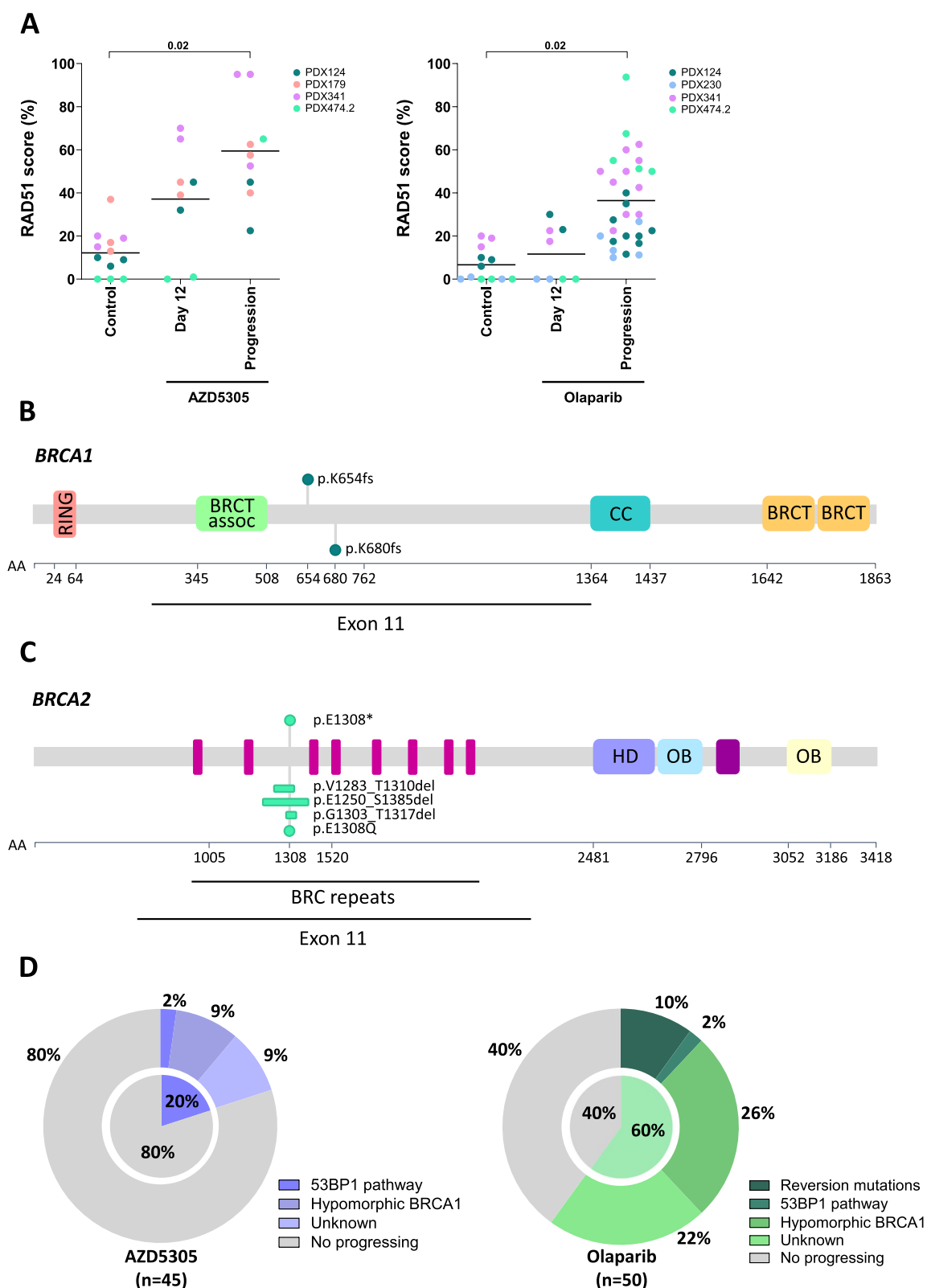
Fig. 3 Mechanisms of resistance to AZD5305 and olaparib in PDXs. **A** Quantification by IF of the RAD51 score (%) in tumors that progressed under treatment with either PARPi, compared to tumors treated in the response phase (day 12) and untreated controls. *p* values are shown. Location of pathogenic (up) and reversion (down) mutations on the domain structure of **B** *BRCA1* and **C** *BRCA2*. Each dot represents a patient. **D** Fraction of resistance mechanisms detected in individual tumors that had progressed to AZD5305 and olaparib in purple and green, respectively

Herencia-Ropero *et al. Genome Medicine* (2024) 16:107

Page 10 of 17

a *BRCA1* reversion mutation (Additional file 9: Fig. S5A). Moreover, increased levels of BRCA1 foci in the tumors that had progressed on either PARPi were accompanied by increased levels of RAD51 foci, suggesting that there was a concomitant enhanced HRR functionality ($R^2 = 0.24$, $p = 0.01$, Additional file 9: Fig. S5B). We further observed that the increased expression of *BRCA1* Δ11q-splicing mRNA isoforms was not a common mechanism leading to enhanced BRCA1 foci formation, since only three out of 17 (18%) olaparib-progressing tumors with high levels of BRCA1 foci showed transcriptional upregulation of the *BRCA1* Δ11q isoform (Additional file 9: Fig. S5C and S5D).

Finally, we reviewed the presence of mutations on other PARPi resistance factors such as *TP53BP1*, *RIF1*, *PAXIP1*, and members of the Shieldin complex. We noted that one AZD5305-progressing tumor from PDX124 showed lack of 53BP1 nuclear foci formation, without evidence of tumor mutation (Additional file 8: Fig. S4A). In addition, a mutation in *SHLD3* was found in an additional olaparib-progressing tumor from PDX124 at an allele frequency of 0.2, which was accompanied by low expression of *SHLD3* by RNA sequencing (Additional file 6: Supplementary Table S4 and Additional file 10: Supplementary Table S5). No other alterations in genes associated with PARPi resistance were identified (Additional file 11: Supplementary Table S6).

In summary, these data show that restoration of HRR is commonly associated with resistance to PARPi, and that the most prevalent mechanisms are *BRCA1/2* reversion mutations and the accumulation of hypomorphic BRCA1.

AZD5305 inhibits PARylation and enhances biomarkers of DNA damage and replication stress

We next analyzed potential differences in the mode of action of PARP1 selective vs. PARP1/2 inhibition in an attempt to identify the key mechanism leading to the incremental response observed with AZD5305, compared to olaparib. Firstly, we analyzed the effect on protein poly(ADP-ribosylation) (PARylation) after the initial dose and after 12 days of treatment with both compounds in a subset of models. Inhibition of PARylation was observed at 2 h after dosing in both AZD5305-resistant and -sensitive tumors treated with either AZD5305 or olaparib (Additional file 12: Fig. S6A). However, while treatment with AZD5305 inhibited PARylation by > 90% over the period of 24 h post-dose, PARylation levels recovered to 56% by 24 h after treatment with olaparib (Additional file 12: Fig. S6B). Likewise to inhibition of PARylation at 2 h after dosing, DNA damage accumulation, as measured by γ-H2AX nuclear foci, increased upon treatment with both PARPi in AZD5305-sensitive

and resistant models (Fig. 4A). AZD5305 is also a potent and selective PARP1 trapper [29], likely leading to the accumulation of replication stress derived from stalled and collapsed DNA replication forks [18, 50]. In this sense, phosphorylation of RPA2 on Ser-4/8 (pRPA) is a good marker of collapsed replication forks [51]. Higher levels of pRPA were observed in AZD5305-sensitive PDXs treated with AZD5305 compared to baseline, with no significant difference in AZD5305-resistant models or olaparib-treated, suggesting a poorer capacity of the sensitive models resolving the replication stress produced by PARP1 trapped on chromatin (Fig. 4B). Finally, we quantified DNA-containing micronuclei as marker of genomic instability due to mitotic progression following DNA damage [52]. Interestingly, treatment with AZD5305 significantly increased micronuclei only in AZD5305-sensitive models (Fig. 4C). In summary, the PARP1 selective inhibitor AZD5305 induces more replication stress and genomic instability than the PARP1/2 inhibitor olaparib in PARPi-sensitive tumors.

Treatment with AZD5305 elicits profound and durable responses in combination with carboplatin or an ATRi in PARPi-resistant models

The addition of PARPi to platinum salts has demonstrated combination benefit in select preclinical models [29, 53, 54]. This combination has also been investigated in the clinic, albeit with challenges to demonstrate safety, or efficacy when using PARPi with low trapping capacity or a gap schedule [55–58]. In this sense, Illuzzi et al. demonstrated that treatment with AZD5305 in combination with carboplatin in preclinical models results in rapid recovery of red blood cell parameters, contrary to the sustained loss observed with olaparib plus carboplatin [29]. We therefore investigated whether the antitumor activity of AZD5305 could be increased by adding carboplatin in a subset of six PDXs with a range of responses to AZD5305 (Fig. 5A). AZD5305 plus carboplatin induced tumor regression (CR) in two models with primary resistance to both PARPi, namely PDX127 and PDX341, as well as in one model sensitive to AZD5305 (PDX124). Durable responses were observed upon combination treatment in PDX127 (Additional file 13: Fig. S7A). However, AZD5305 plus carboplatin did not induce tumor regression in any of the PDXs with acquired resistance to olaparib (PDX474.2OR2, PDX474.7, or PDX230OR5).

Similar to carboplatin, ATR inhibition has the potential to synergize with PARPi since trapped PARP1 can lead to replication fork stalling, which requires ATR for resolution [18, 21]. Thus, we explored the antitumor activity of AZD5305 in combination with the ATRi ceralasertib (AZD6738) in a subset of five PDXs. AZD5305 plus AZD6738 induced tumor regression (CR) in PDX127, a
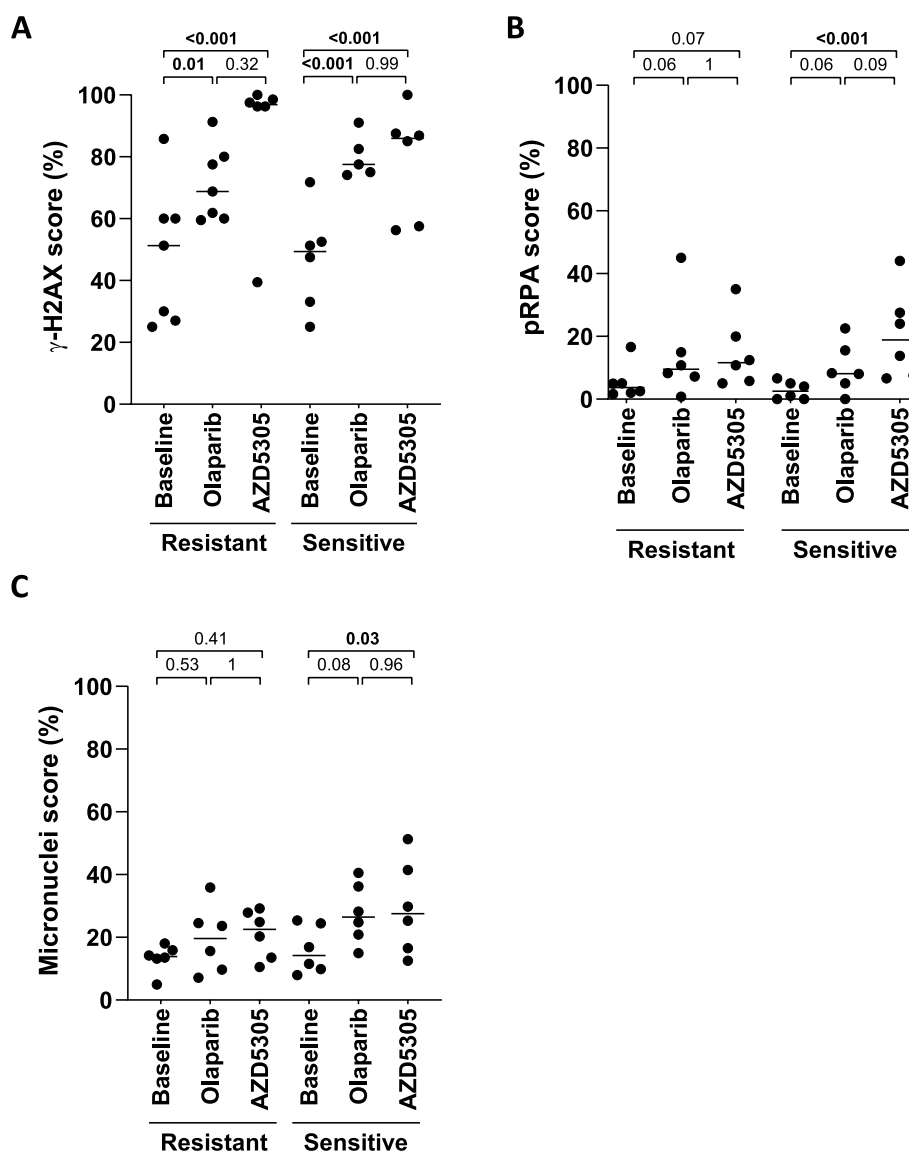
Fig. 4 Biomarkers of DNA damage and replication stress in PDX models. Quantification of the percentage of tumor cells **A** in S/G2-phase (geminin-positive) with γ-H2AX nuclear foci, **B** in S/G2-phase (geminin-positive) with phospho-RPA nuclear foci, or **C** with at least one micronucleus in AZD5305-resistant ($n=6$) and sensitive ($n=6$) available PDX models, untreated or treated for 12 days with olaparib 100 mg/kg and AZD5305 1 mg/kg. Black lines indicate the biomarker mean of each group. *p* values (linear mixed-effects models) are indicated with significant values labeled in bold

(See figure on next page.)
Fig. 5 Antitumor activity of AZD5305 as single agent and in combination with other DNA damaging agents. Waterfall plots showing the antitumor activity of AZD5305 with **A** carboplatin as single agent and in combination in $n=6$ PDX models and with **B** AZD6738 as single agent and in combination in $n=5$ models, measured as percentage of tumor volume change, compared with the tumor volume on day 1. Each bar indicates the mean and SEM of at least three biological replicates (open circles). The mean of control tumors ($n \geq 3$) is represented with solid circles. +20%, −30%, and −95% are marked by dotted lines to indicate the range of PD, SD, PR, and CR, respectively. The lower box summarizes the RAD51 score (%), the specific gene alteration harbored by each model, the cancer type, and previous treatment history with DDR drugs in the "Early"-stage vs. "Metastatic" disease setting. Rev, reversion mutation; DDR, DNA damage repair. *p* values, pairwise Wilcoxon test corrected for multiple testing
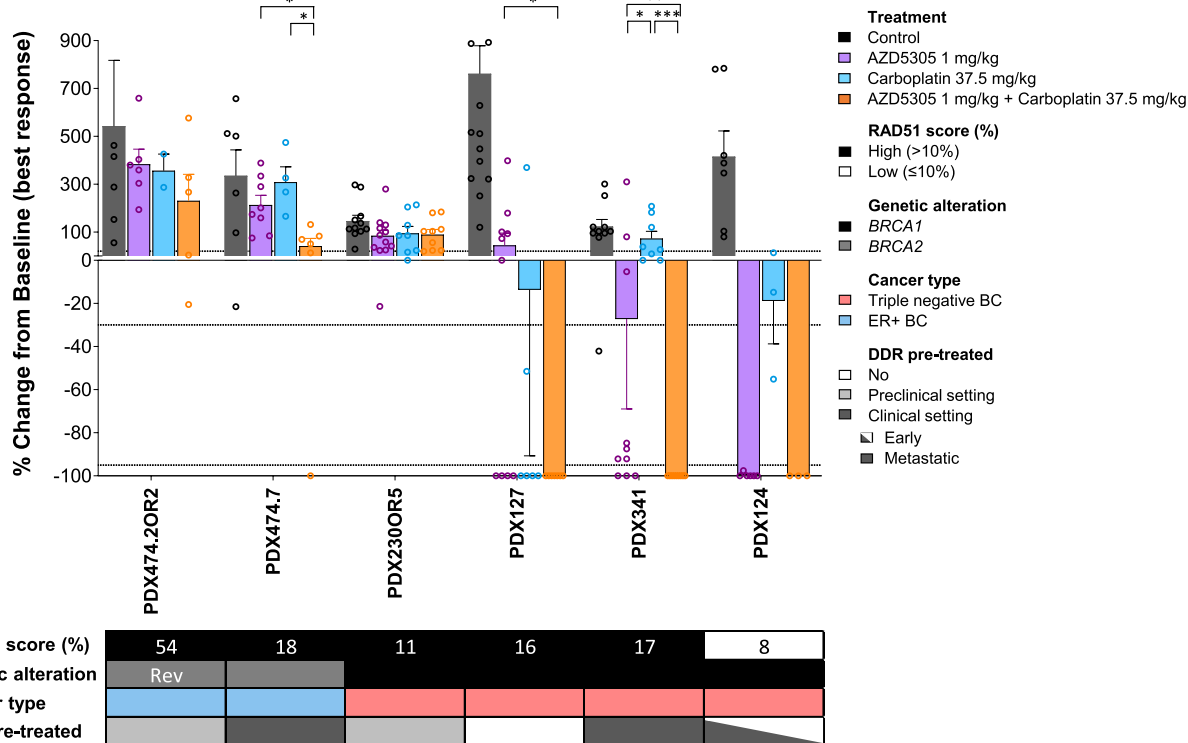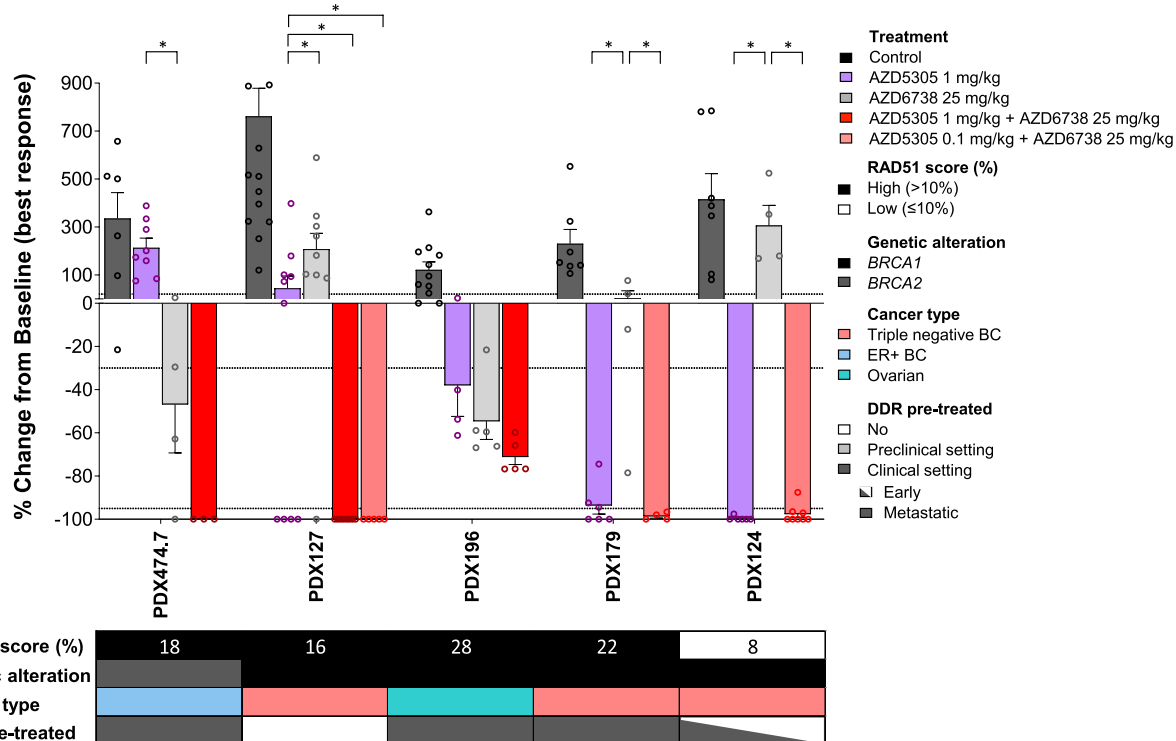
Fig. 5 (See legend on previous page.)

model with primary resistance to either PARPi (Additional file 13: Fig. S7B). Interestingly, this combination also resulted in CR in PDX474.7, a model obtained after the clinical progression to talazoparib, and that was not responsive to the combination of AZD5305 plus carboplatin. Ceralasertib increased the magnitude and the duration of response in three AZD5305-sensitive models (PDX124, PDX179, and PDX196) without compromising tolerability (Fig. 5B and Additional file 13: S7B–G). Of note, the combination arms for PDX124, PDX179, and PDX127 were conducted with a tenfold lower dose of AZD5305 and led to complete response. Taken together, these results demonstrate that response to AZD5305 can be improved by combining it with carboplatin or an ATRi.

Discussion

First-generation PARPi have been shown to be effective in tumors with alterations in the HRR pathway leading to their approval and use in the clinic in tumor types where *BRCA1/2* mutations are prevalent [1–14]. However, and despite this practice-changing discovery, the emergence of drug resistance remains a clinical limitation and thus, more efficient therapeutic options are needed [17, 19, 59]. AZD5305 is a potent and highly selective PARP1 inhibitor and trapper that has been previously shown to have a greater target engagement and antiproliferative activity than first-generation PARP inhibitors in cells with HRD [29]. Here, we demonstrate that AZD5305 elicits more potent and durable antitumor activity in vivo than a first-generation PARPi across a panel of *BRCA1/2*- and *PALB2*-associated PDX models. We also confirm that PARPi-sensitive PDX models show lower RAD51 foci levels than PARPi-resistant and that enhancement of HRR functionality is ubiquitous in models of acquired resistance. We further show that the addition of carboplatin or an ATR inhibitor overcomes PARPi resistance in PDX models.

PARP1 selective inhibitors are expected to differentiate from first-generation PARP1/2 inhibitors in several aspects. Firstly, it would be desirable that they result in an improved clinical response, being able to overcome resistance to former drugs by providing a wider therapeutic window, and second, that they offer the opportunity to be more easily combined with other DNA damaging agents to overcome drug resistance. In addition, understanding the mechanisms leading to the emergence of resistance is a key aspect to rationally design subsequent therapies.

Our study suggests that AZD5305 as single agent does not exhibit antitumor activity in preclinical models of acquired resistance to the first-generation PARP1/2i olaparib or talazoparib, where resistance involved

restoration of HRR. Also, AZD5305 did not show antitumor activity in a pancreatic cancer model that does not harbor biallelic inactivation in *PALB2*, nor functional HRD by RAD51 foci. This is consistent with the lower frequency of biallelic inactivation and HRD in tumors harboring *PALB2* mutations compared to those with *BRCA1/2* mutations in breast cancer (67% vs. 85%) and pan-cancer [60–62]. It also highlights the need to identify biallelic *PALB2* inactivation or functional HRD by RAD51 foci in PALB2-associated BC for the personalization of PARPi [37]. Nonetheless, AZD5305 showed superior activity to olaparib in some models which might represent tumors of intermediate HRR capacity (PDX179, PDX341). We reason that residual HRR is sufficient to limit responses to olaparib, but that can be overwhelmed by the greater pharmacodynamic, PARP1 trapping and DNA damaging properties of AZD5305, leading to responses. It is interesting to note that, in the phase I/IIa PETRA trial (NCT04644068), preliminary results have been reported and antitumor activity was observed both in patients who were PARPi naïve and in those who had received a prior PARPi-containing treatment, although had not necessarily progressed on PARPi [63]. Another interesting aspect of our results is the observation that treatment with AZD5305 delivers a higher complete response rate and longer-term responses as single agent than olaparib. This would be potentially relevant in the advanced and in the early breast cancer setting, where *BRCA1/2* carriers could potentially achieve further overall survival benefit as it has already been demonstrated for olaparib [10].

Mechanistically, AZD5305 induces DNA damage and elicits a replication stress response along with an increase in markers of genomic instability, measured with the induction of γ-H2AX, pRPA, and DNA-containing micronuclei, respectively. This is consistent with cell line data showing selective and more potent PARP1 trapping at the low nanomolar range of AZD5305, compared to olaparib [29]. We acknowledge that the acute measurements obtained from the short-term pharmacodynamic experiments conducted in the PDXs may not fully capture all the longer-term effects that AZD5305 elicits on tumor cells and translates into the observed preclinical benefit. Also, the accumulation of genomic instability produced by treatment with DNA damaging agents such as PARPi results in the activation of the STING pathway, promoting an innate immune response [64]. In this sense, further research is needed to characterize the antitumor immune response elicited after treatment with AZD5305 in syngeneic mouse models and also in human samples, without the inherent limitations of mouse experiments.

Reversion mutations that restore the open reading frame of the *BRCA1* and *BRCA2* genes have emerged as

a recurrent mechanism to restore HRR function leading to PARPi resistance. In the OlympiAD trial, involving *BRCA1/2* mutation carriers with metastatic breast cancer treated until disease progression with olaparib, reversion mutations were rarely detected in circulating tumor DNA (ctDNA) at baseline (3%), but they were acquired at disease progression in a substantial amount of patients (40%) [65]. Our preclinical data suggest that models harboring baseline reversion mutations are intrinsically resistant to AZD5305. Also importantly, acquired resistance to PARP1 selective inhibition occurs in a smaller fraction of tumors compared to PARP1/2 inhibition, and neither *BRCA1/2* reversion mutations nor *TP53BP1* mutations were observed upon progression to AZD5305, probably due to the relatively small sample size used in this study. We speculate that *BRCA1/2* reversion mutations might become more prevalent in the near future in breast cancer patients, based on the current treatment regimens that include platinum in the early setting and the observation of relatively high frequency of *BRCA1/2* reversion mutations vs. *TP53BP1* mutations in patients who received platinum drugs [66]. Our preclinical models also identify the presence of other mechanisms of PARPi resistance that restore HRR functionality, including BRCA1/2 hypomorphs and loss of 53BP1 pathway components that are all being captured with the RAD51 foci assay [37, 45, 46].

Given that some of these mechanisms remain elusive and the small size of the PDX panel, we cannot fully elaborate on response biomarkers to treatment with AZD5305 plus platinum or AZD5305 plus ATRi combinations, as done previously with olaparib combinations [21]. Nonetheless, we observed that PDXs that responded to AZD5305 plus carboplatin (PDX127 and PDX341) had a primary resistance or heterogeneous response to PARPi, respectively, and harbor defects in the 53BP1 pathway [43]. In contrast, models that had acquired resistance to olaparib were prone to re-express BRCA2 variants (PDX474.2OR2 and PDX474.7) and were resistant to AZD5305 plus carboplatin. Also interestingly, the combination with the ATRi was effective in one model with acquired resistance to olaparib that was not rescued by the combination of AZD5305 plus carboplatin (PDX474.7). Therefore, our data warrants further investigation for this combination in the clinic. The PETRA trial will inform about safety and signs of AZD5305 activity in advanced patients harboring *BRCA1/2*, *PALB2*, or *RAD51C/D* mutations [63].

Conclusions

In summary, our data show that the PARP1 selective inhibitor AZD5305 is a more potent anticancer therapy than a first-generation PARPi. We demonstrate that AZD5305 elicits improved and sustained response in vivo in tumors with HRR mutations both alone or in combination with platinum salts or an ATRi. These in vivo results support previously described in vitro data and the development of new treatment combinations in the clinic.

Abbreviations

PARPi	Poly (ADP-ribose) polymerase inhibitors
PDX	Patient-derived xenograft
DSB	Double strand break
HRR	Homologous recombination repair
HRD	Homologous recombination deficiency
BC	Breast cancer
TNBC	Triple negative breast cancer
FFPE	Formalin-fixed paraffin embedded
mRECIST	Modified Response Evaluation Criteria in Solid Tumors
CR	Complete response
PR	Partial response
SD	Stable disease
PD	Progressive disease
pCRR	Preclinical complete response rate
pORR	Preclinical overall response rate
pCBR	Preclinical benefit rate
pPFS	Preclinical progression-free survival
pTTP	Preclinical time to progression
qPCR	Quantitative polymerase chain reaction
DDR	DNA damage repair
IF	Immunofluorescence
CI	Confidence intervals
gsLOH	Gene-specific loss of heterozygosity
p.o.	Orally
i.p.	Intraperitoneally
MMEJ	Microhomology mediated end joining
ctDNA	Circulating tumor DNA

Supplementary Information

Additional file 1: Supplementary Table S1. Clinical information.

Additional file 2: Supplementary Table S2. Molecular characteristics of the PDX cohort.

Additional file 3: Supplementary Table S3. Whole-exome sequencing data of the PDX cohort.

Additional file 4: Fig. S1. Characterization of mechanisms of resistance to PARPi in PDX models.

Additional file 5: Fig. S2 Analysis of response to AZD5305 and olaparib in PDXs.

Additional file 6: Supplementary Table S4 Molecular characteristics of tumors with acquired resistance to PARPi.

Additional file 7: Fig. S3 Assessment of the functional HRD status by RAD51 foci.

Additional file 8: Fig. S4 Characterization of genetic-based mechanisms of resistance to PARPi in PDXs.

Additional file 9: Fig. S5 Characterization of the protein-based mechanisms of resistance to PARPi.

Additional file 10: Supplementary Table S5 RNA-sequencing data of the PDX cohort.

Additional file 11: Supplementary Table S6 Mechanisms of resistance to PARPi evaluated in our cohort of PDX models.

Additional file 12: Fig. S6 Analysis of the catalytic activity of PARPi in PDXs.

Additional file 13: Fig. S7 Antitumor activity of AZD5305 in combination with DDR drugs.

Availability of data and materials
DNA and RNA sequencing data supporting the findings of this study are available in the supplementary information files of the article.

Declarations

Ethics approval and consent to participate
Fresh tumor samples from cancer patients were collected for implantation into nude mice under a protocol approved by the Ethics Committee for Clinical Research (PR(AG)484/2017) and an associated written informed consent. Procedures involving human specimens were conducted according to the principles of the Helsinki Declaration. Experiments were conducted following the European Union's animal care directive (2010/63/EU) and were approved by the Ethical Committee of Animal Experimentation of the Vall d'Hebron Research Institute. All patients provided written informed consent to participate in the study.

Consent for publication
Not applicable.

Competing interests
ALG, VS, and JB are co-inventors of a patent related to this work (WO2019122411A1). We report research grants from AstraZeneca (VS) and personal fees and/or nonfinancial support from AstraZeneca (JB, VS), Pfizer (JB), and GSK (VS). ADS, FJCN, ST, LT, EL, AL, ALG, JF, MJOC, and MA are full time-time employees and shareholders at AZ. The remaining authors declare that they have no competing interests. The PARPi and ATRi used in this study were provided by AstraZeneca.

Author details
[1]Experimental Therapeutics Group, Vall d'Hebron Institute of Oncology (VHIO), Vall d'Hebron Barcelona Hospital Campus, Carrer Natzaret 115-117, 08035 Barcelona, Spain. [2]Department of Biochemistry and Molecular Biology, Autonomous University of Barcelona, Barcelona, Spain. [3]Oncology R&D, AstraZeneca, Cambridge, UK. [4]Hereditary Cancer Genetics Group, Vall d'Hebron Institute of Oncology (VHIO), Vall d'Hebron Barcelona Hospital Campus, Carrer Natzaret 115-117, 08035 Barcelona, Spain. [5]Programa de doctorat en Biomedicina, Universitat de Barcelona, Barcelona, Spain. [6]Oncology Data Science Group, Vall d'Hebron Institute of Oncology (VHIO), Vall d'Hebron Barcelona Hospital Campus, Barcelona, Spain. [7]Medicine Genetics Group, Vall d'Hebron Institut de Recerca (VHIR), Vall d'Hebron Barcelona Hospital Campus, Barcelona, Spain. [8]Department of Clinical and Molecular Genetics, Vall d'Hebron Barcelona Hospital Campus, Barcelona, Spain. [9]Growth Factors Group, Vall d'Hebron Institute of Oncology (VHIO), Vall d'Hebron Barcelona Hospital Campus, Barcelona, Spain. [10]Centro de Investigación Biomédica en Red de Cáncer, Monforte de Lemos, Madrid, Spain. [11]Epigenetics Group, Josep Carreras Leukaemia Research Institute, Barcelona, Spain. [12]Preclinical and Translational Research Program, Vall d'Hebron Institute of Oncology (VHIO), Vall d'Hebron Barcelona Hospital Campus, Barcelona, Spain. [13]Gastrointestinal and Endocrine Tumor Unit, Vall d'Hebron Institute of Oncology (VHIO), Vall d'Hebron Barcelona Hospital Campus, Barcelona, Spain. [14]Molecular Oncology Group, Vall d'Hebron Institute of Oncology (VHIO), Vall d'Hebron Barcelona Hospital Campus, Barcelona, Spain. [15]Departament of Medicine and Life Sciences, Pompeu Fabra University, Barcelona, Spain. [16]Catalan Institution for Research and Advanced Studies, ICREA, Barcelona, Spain. [17]Cancer Research Program, The Hospital del Mar Research Institute, Barcelona, Spain. [18]Department of Medical Oncology, Vall d'Hebron Barcelona Hospital Campus, Autonomous University of Barcelona, Barcelona, Spain.

References
1. Ledermann J, Harter P, Gourley C, et al. Olaparib maintenance therapy in patients with platinum-sensitive relapsed serous ovarian cancer: a preplanned retrospective analysis of outcomes by BRCA status in a randomised phase 2 trial. Lancet Oncol. 2014;15(8):852–61.
2. Ledermann JA, Harter P, Gourley C, et al. Overall survival in patients with platinum-sensitive recurrent serous ovarian cancer receiving olaparib maintenance monotherapy: an updated analysis from a randomised, placebo-controlled, double-blind, phase 2 trial. Lancet Oncol. 2016;17(11):1579–89.
3. Mirza MR, Monk BJ, Herrstedt J, et al. Niraparib maintenance therapy in platinum-sensitive, recurrent ovarian cancer. N Engl J Med. 2016;375(22):2154–64.
4. Coleman RL, Oza AM, Lorusso D, et al. Rucaparib maintenance treatment for recurrent ovarian carcinoma after response to platinum therapy (ARIEL3): a randomised, double-blind, placebo-controlled, phase 3 trial. Lancet. 2017;390(10106):1949–61.
5. Moore K, Colombo N, Scambia G, et al. Maintenance olaparib in patients with newly diagnosed advanced ovarian cancer. N Engl J Med. 2018;379(26):2495–505.
6. Ray-Coquard I, Pautier P, Pignata S, et al. Olaparib plus bevacizumab as first-line maintenance in ovarian cancer. N Engl J Med. 2019;381(25):2416–28.
7. Gonzalez-Martin A, Pothuri B, Vergote I, et al. Niraparib in patients with newly diagnosed advanced ovarian cancer. N Engl J Med. 2019;381(25):2391–402.
8. Robson M, Im SA, Senkus E, et al. Olaparib for metastatic breast cancer in patients with a germline BRCA mutation. N Engl J Med. 2017;377(6):523–33.
9. Litton JK, Rugo HS, Ettl J, et al. Talazoparib in patients with advanced breast cancer and a germline BRCA mutation. N Engl J Med. 2018;379(8):753–63.

10. Tutt ANJ, Garber JE, Kaufman B, et al. Adjuvant olaparib for patients with BRCA1- or BRCA2-mutated breast cancer. N Engl J Med. 2021;384(25):2394–405.

11. Golan T, Hammel P, Reni M, et al. Maintenance olaparib for germline BRCA-mutated metastatic pancreatic cancer. N Engl J Med. 2019;381(4):317–27.

12. de Bono J, Mateo J, Fizazi K, et al. Olaparib for metastatic castration-resistant prostate cancer. N Engl J Med. 2020;382(22):2091–102.

13. Abida W, Patnaik A, Campbell D, et al. Rucaparib in men with metastatic castration-resistant prostate cancer harboring a BRCA1 or BRCA2 gene alteration. J Clin Oncol. 2020;38(32):3763–72.

14. Clarke NW, Armstrong AJ, Thiery-Vuillemin A, et al. Abiraterone and olaparib for metastatic castration-resistant prostate cancer. NEJM Evid. 2022;1(9):EVIDoa2200043.

15. Bryant HE, Schultz N, Thomas HD, et al. Specific killing of BRCA2-deficient tumours with inhibitors of poly (ADP-ribose) polymerase. Nature. 2005;434(7035):913–7.

16. Farmer H, McCabe N, Lord CJ, et al. Targeting the DNA repair defect in BRCA mutant cells as a therapeutic strategy. Nature. 2005;434(7035):917–21.

17. Lord CJ, Ashworth A. PARP inhibitors: synthetic lethality in the clinic. Science. 2017;355(6330):1152–8.

18. Pommier Y, O'Connor MJ, de Bono J. Laying a trap to kill cancer cells: PARP inhibitors and their mechanisms of action. Sci Transl Med. 2016;8(362):362ps317.

19. Francica P, Rottenberg S. Mechanisms of PARP inhibitor resistance in cancer and insights into the DNA damage response. Genome Med. 2018;10(1):101.

20. O'Connor MJ. Targeting the DNA damage response in cancer. Mol Cell. 2015;60(4):547–60.

21. Serra V, Wang AT, Castroviejo-Bermejo M, et al. Identification of a molecularly-defined subset of breast and ovarian cancer models that respond to WEE1 or ATR inhibition, overcoming PARP inhibitor resistance. Clin Cancer Res. 2022;28(20):4536–50.

22. Wethington SL, Shah PD, Martin L, et al. Combination ATR (ceralasertib) and PARP (olaparib) inhibitor (CAPRI) trial in acquired PARP inhibitor-resistant homologous recombination-deficient ovarian cancer. Clin Cancer Res. 2023;29(15):2800–7.

23. LaFargue CJ, Dal Molin GZ, Sood AK, Coleman RL. Exploring and comparing adverse events between PARP inhibitors. Lancet Oncol. 2019;20(1):e15–28.

24. Murai J, Huang SY, Das BB, et al. Trapping of PARP1 and PARP2 by clinical PARP inhibitors. Cancer Res. 2012;72(21):5588–99.

25. Ronson GE, Piberger AL, Higgs MR, et al. PARP1 and PARP2 stabilise replication forks at base excision repair intermediates through Fbh1-dependent Rad51 regulation. Nat Commun. 2018;9(1):746.

26. Farres J, Martin-Caballero J, Martinez C, et al. Parp-2 is required to maintain hematopoiesis following sublethal gamma-irradiation in mice. Blood. 2013;122(1):44–54.

27. Farres J, Llacuna L, Martin-Caballero J, et al. PARP-2 sustains erythropoiesis in mice by limiting replicative stress in erythroid progenitors. Cell Death Differ. 2015;22(7):1144–57.

28. Johannes JW, Balazs A, Barratt D, et al. Discovery of 5-4-[(7-ethyl-6-oxo-5,6-dihydro-1,5-naphthyridin-3-yl)methyl]piperazin-1-yl-N-methylpyridine-2-carboxamide (AZD5305): a PARP1-DNA trapper with high selectivity for PARP1 over PARP2 and other PARPs. J Med Chem. 2021;64(19):14498–512.

29. Illuzzi G, Staniszewska AD, Gill SJ, et al. Preclinical characterization of AZD5305, a next-generation, highly selective PARP1 inhibitor and trapper. Clin Cancer Res. 2022;28(21):4724–36.

30. Ahdesmaki MJ, Gray SR, Johnson JH, Lai Z. Disambiguate: an open-source application for disambiguating two species in next generation sequencing data from grafted samples. F1000Res. 2016;5:2741.

31. Lai Z, Markovets A, Ahdesmaki M, et al. VarDict: a novel and versatile variant caller for next-generation sequencing in cancer research. Nucleic Acids Res. 2016;44(11):e108.

32. Janssen K, Duran-Romana R, Bottu G, et al. SNPeffect 5.0: large-scale structural phenotyping of protein coding variants extracted from next-generation sequencing data using AlphaFold models. BMC Bioinformatics. 2023;24(1):287.

33. Patro R, Duggal G, Love MI, Irizarry RA, Kingsford C. Salmon provides fast and bias-aware quantification of transcript expression. Nat Methods. 2017;14(4):417–9.

34. Love MI, Huber W, Anders S. Moderated estimation of fold change and dispersion for RNA-seq data with DESeq2. Genome Biol. 2014;15(12):550.

35. Schmittgen TD, Livak KJ. Analyzing real-time PCR data by the comparative C(T) method. Nat Protoc. 2008;3(6):1101–8.

36. Colombo M, Lopez-Perolio I, Meeks HD, et al. The BRCA2 c.68–7T > A variant is not pathogenic: a model for clinical calibration of spliceogenicity. Hum Mutat. 2018;39(5):729–41.

37. Castroviejo-Bermejo M, Cruz C, Llop-Guevara A, et al. A RAD51 assay feasible in routine tumor samples calls PARP inhibitor response beyond BRCA mutation. EMBO Mol Med. 2018;10(12):e9172.

38. Ballabeni A, Zamponi R, Moore JK, Helin K, Kirschner MW. Geminin deploys multiple mechanisms to regulate Cdt1 before cell division thus ensuring the proper execution of DNA replication. Proc Natl Acad Sci U S A. 2013;110(30):E2848–2853.

39. Benjamini Y, Hochberg Y. Controlling the false discovery rate: a practical and powerful approach to multiple testing. J R Statist Soc B. 1995;57(1):289–300.

40. Bates D, Mächler M, Bolker B, Walker S. Fitting linear mixed-effects models using lme4. J Stat Softw. 2015;67(1):1–48.

41. Therneau T. coxme: mixed effects Cox models. R package version 2.2–18.1. 2022. https://cran.r-project.org/web/packages/coxme/coxme.pdf.

42. Team RC. R: a language and environment for statistical computing. R Foundation for Statistical Computing. 2023. https://www.R-project.org/.

43. Dev H, Chiang TW, Lescale C, et al. Shieldin complex promotes DNA end-joining and counters homologous recombination in BRCA1-null cells. Nat Cell Biol. 2018;20(8):954–65.

44. Park PH, Yamamoto TM, Li H, et al. Amplification of the mutation-carrying BRCA2 allele promotes RAD51 loading and PARP inhibitor resistance in the absence of reversion mutations. Mol Cancer Ther. 2020;19(2):602–13.

45. Cruz C, Castroviejo-Bermejo M, Gutierrez-Enriquez S, et al. RAD51 foci as a functional biomarker of homologous recombination repair and PARP inhibitor resistance in germline BRCA-mutated breast cancer. Ann Oncol. 2018;29(5):1203–10.

46. Pellegrino B, Herencia-Ropero A, Llop-Guevara A, et al. Preclinical in vivo validation of the RAD51 test for identification of homologous recombination-deficient tumors and patient stratification. Cancer Res. 2022;82(8):1646–57.

47. Wang Y, Bernhardy AJ, Cruz C, et al. The BRCA1-Delta11q alternative splice isoform bypasses germline mutations and promotes therapeutic resistance to PARP inhibition and cisplatin. Cancer Res. 2016;76(9):2778–90.

48. Pettitt SJ, Frankum JR, Punta M, et al. Clinical BRCA1/2 reversion analysis identifies hotspot mutations and predicted neoantigens associated with therapy resistance. Cancer Discov. 2020;10(10):1475–88.

49. Tobalina L, Armenia J, Irving E, O'Connor MJ, Forment JV. A meta-analysis of reversion mutations in BRCA genes identifies signatures of DNA end-joining repair mechanisms driving therapy resistance. Ann Oncol. 2021;32(1):103–12.

50. Bunting SF, Callen E, Wong N, et al. 53BP1 inhibits homologous recombination in Brca1-deficient cells by blocking resection of DNA breaks. Cell. 2010;141(2):243–54.

51. Glanzer JG, Liu S, Wang L, Mosel A, Peng A, Oakley GG. RPA inhibition increases replication stress and suppresses tumor growth. Cancer Res. 2014;74(18):5165–72.

52. Harding SM, Benci JL, Irianto J, Discher DE, Minn AJ, Greenberg RA. Mitotic progression following DNA damage enables pattern recognition within micronuclei. Nature. 2017;548(7668):466–70.

53. Rottenberg S, Jaspers JE, Kersbergen A, et al. High sensitivity of BRCA1-deficient mammary tumors to the PARP inhibitor AZD2281 alone and in combination with platinum drugs. Proc Natl Acad Sci U S A. 2008;105(44):17079–84.

54. Dellavedova G, Decio A, Formenti L, et al. The PARP1 inhibitor AZD5305 impairs ovarian adenocarcinoma progression and visceral metastases in patient-derived xenografts alone and in combination with carboplatin. Cancer Res Commun. 2023;3(3):489–500.

55. Balmana J, Tung NM, Isakoff SJ, et al. Phase I trial of olaparib in combination with cisplatin for the treatment of patients with advanced breast, ovarian and other solid tumors. Ann Oncol. 2014;25(8):1656–63.

Herencia-Ropero *et al. Genome Medicine*   (2024) 16:107

Page 17 of 17

56. Dieras V, Han HS, Kaufman B, et al. Veliparib with carboplatin and paclitaxel in BRCA-mutated advanced breast cancer (BROCADE3): a randomised, double-blind, placebo-controlled, phase 3 trial. Lancet Oncol. 2020;21(10):1269–82.

57. Loibl S, O'Shaughnessy J, Untch M, et al. Addition of the PARP inhibitor veliparib plus carboplatin or carboplatin alone to standard neoadjuvant chemotherapy in triple-negative breast cancer (BrighTNess): a randomised, phase 3 trial. Lancet Oncol. 2018;19(4):497–509.

58. Abraham JE, Pinilla K, Dayimu A, et al. The PARTNER trial of neoadjuvant olaparib with chemotherapy in triple-negative breast cancer. Nature. 2024. https://doi.org/10.1038/s41586-024-07384-2.

59. Mateo J, Lord CJ, Serra V, et al. A decade of clinical development of PARP inhibitors in perspective. Ann Oncol. 2019;30(9):1437–47.

60. Lee JEA, Li N, Rowley SM, et al. Molecular analysis of PALB2-associated breast cancers. J Pathol. 2018;245(1):53–60.

61. Li A, Geyer FC, Blecua P, et al. Homologous recombination DNA repair defects in PALB2-associated breast cancers. NPJ Breast Cancer. 2019;5:23.

62. Srinivasan P, Bandlamudi C, Jonsson P, et al. The context-specific role of germline pathogenicity in tumorigenesis. Nat Genet. 2021;53(11):1577–85.

63. Yap TA, Im S-A, Schram AM, et al. PETRA: a first-in-class, first-in-human trial of the next-generation PARP1-selective inhibitor AZD5305 in patients with BRCA1/2, PALB2 or RAD51C/D mutations. New Orleans, USA: In. AACR annual meeting; 2022.

64. Parkes EE, Humphries MP, Gilmore E, et al. The clinical and molecular significance associated with STING signaling in breast cancer. NPJ Breast Cancer. 2021;7(1):81.

65. Lukashchuk N, Armenia J, Luis Tobalina T, et al. BRCA reversion mutations mediated by microhomology-mediated end joining (MMEJ) as a mechanism of resistance to PARP inhibitors in ovarian and breast cancer. Chicago, USA: In. ASCO annual meeting; 2022.

66. Harvey-Jones E, Raghunandan M, Robbez-Masson L, et al. Longitudinal profiling identifies co-occurring BRCA1/2 reversions, TP53BP1, RIF1 and PAXIP1 mutations in PARP inhibitor-resistant advanced breast cancer. Ann Oncol. 2024;35(4):364–80.

Publisher's Note